

See discussions, stats, and author profiles for this publication at: <https://www.researchgate.net/publication/305383334>

Platinum-group element abundances and Re-Os isotopic systematics of the upper continental crust through time: Evidence...

Article in *Geochimica et Cosmochimica Acta* · July 2016

DOI: 10.1016/j.gca.2016.07.004

CITATION

1

READS

169

8 authors, including:



Kang Chen

China University of Geosciences

8 PUBLICATIONS 123 CITATIONS

[SEE PROFILE](#)



R. M. Gaschnig

University of Massachusetts Lowell

34 PUBLICATIONS 293 CITATIONS

[SEE PROFILE](#)



Igor S. Puchtel

University of Maryland, College Park

136 PUBLICATIONS 3,166 CITATIONS

[SEE PROFILE](#)



Ming Tang

Rice University

13 PUBLICATIONS 168 CITATIONS

[SEE PROFILE](#)



Available online at www.sciencedirect.com

ScienceDirect

Geochimica et Cosmochimica Acta 191 (2016) 1–16

**Geochimica et
Cosmochimica
Acta**

www.elsevier.com/locate/gca

Platinum-group element abundances and Re–Os isotopic systematics of the upper continental crust through time: Evidence from glacial diamictites

Kang Chen ^{a,b,*}, Richard J. Walker ^b, Roberta L. Rudnick ^{b,1}, Shan Gao ^{a,†},
Richard M. Gaschnig ^{b,2}, Igor S. Puchtel ^b, Ming Tang ^b, Zhao-Chu Hu ^a

^a State Key Laboratory of Geological Processes and Mineral Resources, School of Earth Sciences, China University of Geosciences, Wuhan 430074, China

^b Department of Geology, University of Maryland, College Park, MD 20742, United States

Received 3 November 2015; accepted in revised form 4 July 2016; Available online 14 July 2016

Abstract

The fine-grained matrix of glacial diamictites, deposited periodically by continental ice sheets over much of Earth history, provides insights into the average composition and chemical evolution of the upper continental crust (UCC) (Gaschnig et al., 2016, and references therein). The concentrations of platinum-group elements (PGEs, including Os, Ir, Ru, Pt and Pd) and the geochemically related Re, as well as $^{187}\text{Re}/^{188}\text{Os}$ and $^{187}\text{Os}/^{188}\text{Os}$ ratios, are reported here for globally-distributed glacial diamictites that were deposited during the Mesoarchean, Paleoproterozoic, Neoproterozoic and Paleozoic eras. The medians and averages of PGE concentrations of these diamictite composites decrease from the Mesoarchean to the Neoproterozoic, mimicking decreases in the concentrations of first-row transition elements (Sc, V, Cr, Co and Ni). By contrast, Re concentrations are highly variable with no discernable trend, owing to its high solubility. Assuming these diamictites are representative of average UCC through time, the new data are fully consistent with the previous inference that the Archean UCC contained a greater proportion of mafic–ultramafic rocks relative to younger UCC. Linear regressions of PGEs versus Cr and Ni concentrations in all the diamictite composites from the four time periods are used to estimate the following concentrations of the PGEs in the present-day UCC: $0.059 \pm 0.016 \text{ ng/g Os}$, $0.036 \pm 0.008 \text{ ng/g Ir}$, $0.079 \pm 0.026 \text{ ng/g Ru}$, $0.80 \pm 0.22 \text{ ng/g Pt}$ and $0.80 \pm 0.26 \text{ ng/g Pd}$ (2σ of 10,000 bootstrapping regression results). These PGE estimates are slightly higher than the estimates obtained from loess samples. We suggest this probably results from loess preferentially sampling younger UCC rocks that have lower PGE concentrations, or PGEs being fractionated during loess formation. A Re concentration of $0.25 \pm 0.12 \text{ ng/g}$ (2σ) is obtained from a regression of Re versus Mo. From this, time-integrated $^{187}\text{Re}/^{188}\text{Os}$ and $^{187}\text{Os}/^{188}\text{Os}$ ratios for the UCC are calculated, assuming an average UCC residence duration of $\sim 2.0 \text{ Ga}$, yielding ratios of 20 ± 12 and 0.80 ± 0.38 (2σ), respectively.

© 2016 Elsevier Ltd. All rights reserved.

Keywords: Platinum-group elements; Re–Os isotopes; Glacial diamictite; Secular variation; Upper continental crust

* Corresponding author at: State Key Laboratory of Geological Processes and Mineral Resources, School of Earth Sciences, China University of Geosciences, Wuhan 430074, China.

E-mail address: kangchen@cug.edu.cn (K. Chen).

† Deceased.

¹ Present address: Department of Earth Science, University of California, Santa Barbara, CA 93106-9630, United States.

² Present address: School of Earth and Atmospheric Sciences, Georgia Institute of Technology, Atlanta 30332-0340, United States.

1. INTRODUCTION

Quantification of the average composition of the continental crust with associated uncertainties, and recognition of secular compositional changes are critical for understanding the origin, differentiation and evolution of the continents. Among the three commonly-defined layers of the continental crust (upper, middle and lower), the upper continental crust (UCC) is the most accessible region and its chemical composition has been the focus of numerous studies ([Rudnick and Gao, 2003](#), and references therein; [Kamber et al., 2005](#); [Hu and Gao, 2008](#); [Gaschnig et al., 2016](#)). The average abundances of the major elements and some trace elements (most of the transition elements, Rb, Sr, Y, Zr, Nb, Ba, rare earth elements, Hf, Ta, Pb, Th and U) in the UCC are generally well known, with most estimates falling within a 20% deviation of the averages of all estimates. Other element abundances are less well constrained, especially the halogens, S, Ge, As, Se, In, Sn, Au, Re and platinum-group elements (PGEs, including Os, Ir, Ru, Rh, Pt and Pd), where estimates of average UCC can vary by factors of two or more. This study seeks to provide new constraints on the average abundances of the PGEs and the geochemically related Re, as well as Re–Os isotopic systematics in the UCC through time.

Owing to their highly siderophile and chalcophile nature, the PGEs tend to partition strongly into metallic and sulfide phases, and as a consequence, ~98% of the Earth's PGEs are estimated to be in the core ([McDonough and Sun, 1995](#); [McDonough, 2003](#)). Accordingly, PGE concentrations in the silicate Earth are typically low (low ng/g to pg/g range). In addition, PGEs are often concentrated in minute accessory phases, which may be heterogeneously distributed within sample powder aliquots (giving rise to the so-called “nugget effect”, [Ravizza and Pyle, 1997](#)) so that multiple analyses of the same sample powders may yield concentrations that vary beyond the precision of a single measurement. Both of these factors present challenges to estimating PGE abundances in the UCC.

Rhenium is a trace element that is geochemically similar to the PGEs in that it is strongly siderophile and can also be chalcophile. ^{187}Re decays to ^{187}Os (half-life = 4.16×10^{10} y), providing a radiogenic isotopic system that is useful for dating melt depletion events in the mantle (e.g., [Carlson and Irving, 1994](#)), molybdenites (e.g., [Stein et al., 1997](#)) and black shales (e.g., [Ravizza and Turekian, 1989](#)). In addition, during mantle melting, Re typically behaves as a moderately incompatible trace element, whereas Os is strongly compatible. Therefore, average crust has a much higher Re/Os ratio than the mantle ([Shirey and Walker, 1998](#)). Over time the high parent/daughter ratio results in the development of highly radiogenic $^{187}\text{Os}/^{188}\text{Os}$ in crustal rocks that can be used as a tracer for crust–mantle interaction (e.g., [Saal et al., 1998](#)). Characterizing the average Re/Os and $^{187}\text{Os}/^{188}\text{Os}$ ratios of the UCC, is, therefore, critical for mass-balance calculations involving this geochemically important reservoir.

Only a few attempts have previously been made to estimate the PGE and Re abundances, and $^{187}\text{Os}/^{188}\text{Os}$ ratio of the UCC ([Table 1](#), [Fig. 1](#)). Some of these efforts have esti-

mated the UCC PGE abundances by taking the average concentrations in different rock types and weighting them in proportion to the relative surface area over which they are exposed ([Shaw et al., 1976](#); [Gao et al., 1998](#)). Another approach is to use data for fine-grained sediments and sedimentary rocks (e.g., loess and shale) to infer the PGE and Re abundances in the UCC exposed to weathering and erosion ([Esser and Turekian, 1993](#); [Wedepohl, 1995](#); [Peucker-Ehrenbrink and Jahn, 2001](#); [Park et al., 2012](#)). In addition, [Schmidt et al. \(1997a\)](#) used impact melts to estimate the PGE and Re abundances in the upper crust of the Baltic Shield. As shown in [Table 1](#) and [Fig. 1](#), the abundance estimates for Os, Ir and Re fall within a relatively narrow range of ~30%, 50% and ~30% deviation from their average values, respectively. However, Ru, Pt, and Pd estimates obtained from fine-grained sediments and sedimentary rocks ([Wedepohl, 1995](#); [Peucker-Ehrenbrink and Jahn, 2001](#); [Park et al., 2012](#)), are generally lower, in some cases by more than one order of magnitude, compared to averages determined from large area surface sampling ([Gao et al., 1998](#)) and impact melt samples ([Schmidt et al., 1997a](#)). In addition, most of the previous estimates are not accompanied by uncertainties, except for the relatively large uncertainties reported by [Schmidt et al. \(1997a, b\)](#).

In this study, we use precise analytical techniques to determine PGE and Re concentrations, as well as $^{187}\text{Re}/^{188}\text{Os}$ and $^{187}\text{Os}/^{188}\text{Os}$ ratios for globally-distributed glacial diamictites deposited during the Mesoarchean, Paleoproterozoic, Neoproterozoic and Paleozoic eras. The major and trace element concentrations of these individual samples and composite samples (see Section 2) have been reported by [Gaschnig et al. \(2014, 2016\)](#). Our objectives are to: (1) investigate how PGE and Re abundances, as well as Re–Os isotopic systematics changed in the UCC over time, (2) provide new estimates of PGE and Re abundances, as well as $^{187}\text{Re}/^{188}\text{Os}$ and $^{187}\text{Os}/^{188}\text{Os}$ ratios in the present-day UCC, and (3) assess the uncertainty of the new estimates.

2. SAMPLES

About 150 individual diamictite samples were collected globally from four geological eras: the Mesoarchean (~2.9 Ga), Paleoproterozoic (~2.2–2.5 Ga), Neoproterozoic (~0.58–0.75 Ga) and Paleozoic (0.30 and 0.33 Ga) ([Tables A1 and A2](#)). Samples are composed of a fine-grained matrix containing a wide range of clasts with different shapes and sizes. The individual diamictite samples come from 24 stratigraphic units or time periods and, thus, 24 diamictite composites were made, with each composite representing one stratigraphic unit or time period ([Tables A1 and A2](#)). Geological background information about the stratigraphic units and the GPS co-ordinates of the individual samples are reported in [Gaschnig et al. \(2014\)](#).

3. ANALYTICAL TECHNIQUES

Individual diamictites were first broken into smaller fragments using a rock hammer with the sample placed between thick plastic sheets. The fragments were then

Table 1

Estimates of PGE abundances (ng/g) and Re–Os isotopes for the upper continental crust.

References	Shaw et al. (1976)	Esser and Turekian (1993)	Wedepohl (1995)^a	Schmidt et al. (1997a, b)	Gao et al. (1998)	Peucker-Ehrenbrink and Jahn (2001)	Park et al. (2012)	This study^b
Os		0.05		0.03 ± 0.02		0.031		0.059 ± 0.016
Ir	0.02	0.05	0.05	0.03 ± 0.02		0.022	0.022	0.036 ± 0.008
Ru			0.1	1.06 ± 0.4		0.21	0.030	0.079 ± 0.026
Pt			0.4	1.5 ± 0.5	1.5	0.51	0.599	0.80 ± 0.22
Pd			0.4	2 ± 0.5	1.46	0.52	0.526	0.80 ± 0.26
Re		0.4				0.198		0.25 ± 0.12
¹⁸⁷ Os/ ¹⁸⁸ Os		1.92				1.40		0.80 ± 0.38
¹⁸⁷ Re/ ¹⁸⁸ Os		48				35		20 ± 12

^a The raw data, analyzed by G. Hartmann using NiS fire assay followed by Te coprecipitation, have not been published.^b Obtained from regression approach, see Section 5.2.2.

crushed in an alumina ceramic jaw crusher, and clasts larger than ~5 mm in diameter were removed from the chips by hand. The remaining, clast-free chips were powdered in an alumina ceramic swing mill. The composite samples were made from individual samples using equal proportions of sample powder (by mass) for each unit, combining 3 to 16 individual powders for each unit or time period. A “composite tree” is provided in Table A2.

About three grams of powder were spiked with appropriate amounts of ¹⁹⁰Os, ¹⁹¹Ir, ⁹⁹Ru, ¹⁹⁴Pt, ¹⁰⁵Pd and ¹⁸⁵Re enriched isotopes prior to digestion. Digestion was conducted in a mixture of 2.5 mL of triple-distilled, concentrated HCl and 5 mL triple-distilled, concentrated HNO₃ in sealed Pyrex borosilicate Carius tubes heated to 270 °C for 4 days (Puchtel et al., 2014). Upon opening the cooled tubes, Os was extracted from the acid phase into CCl₄ and then back-extracted into concentrated HBr (Cohen and Waters, 1996). This was followed by further purification by microdistillation (Birck et al., 1997). Iridium, Ru, Pt, Pd and Re were separated and purified using anion exchange chromatography (Rehkämper and Halliday, 1997). It has been suggested that some Ru measurements reported in the literature may have been compromised due to the possible presence of Ni-argide interferences (Ravizza and Pyle, 1997; Park et al., 2012). This is especially problematic for the NiS fire assay digestion method, which involves addition of a large amount of Ni that can accompany the PGE fraction through the column chemistry. This is not a problem for the present study because no Ni was added to the samples in the Carius tube digestion method, and Ni from the samples was efficiently separated from the PGE fractions by the column separations used.

Osmium isotopic compositions were measured via negative thermal ionization mass spectrometry (N-TIMS, Creaser et al., 1991) at the University of Maryland (UMD), using a secondary electron multiplier (SEM) detector on a Thermo-Fisher Triton instrument. Purified Os, dissolved in HBr, was loaded onto baked Pt filaments (99.99% purity; Materion), dried down, then covered by a Ba(OH)₂ activator solution. The instrumental mass bias was assessed by correcting to ¹⁹²Os/¹⁸⁸Os = 3.083 (Shirey and Walker, 1998), using the exponential fractionation law. The precision of measured ¹⁸⁷Os/¹⁸⁸Os ratios for each analysis of a

sample or reference material (usually 100 cycles) was typically better than 0.1% ($2\sigma_m$, where σ_m refers to standard deviation of the mean, i.e., the standard deviation divided by the square root of the number of observations). An in-house Johnson-Matthey Os isotope standard reference solution yielded an average ¹⁸⁷Os/¹⁸⁸Os of 0.11374 ± 0.00016 (2σ , $n = 5$, σ refers to standard deviation), comparable to the result of 0.11378 obtained from precise measurements using Faraday cups during the entire analytical campaign on this Triton. The precision and accuracy of sample measurements were determined by replicate analyses of the reference material TDB-1 (CANMET Diabase), which is widely used for low abundance PGE studies (Peucker-Ehrenbrink et al., 2003; Meisel and Moser, 2004a; Ishikawa et al., 2014). Analyses of TDB-1 yielded Os concentrations of 0.146 ± 0.016 (2σ , $n = 5$) ng/g and ¹⁸⁷Os/¹⁸⁸Os of 0.94 ± 0.16 (2σ , $n = 5$) (Table 2). These values are within precision of previously reported values (Table 2). The results of two other reference materials (UB-N and OKUM) are also consistent with values reported in the literature (Table 2). All Os measurements were blank corrected. The average total analytical blank for Os was 0.34 ± 0.44 (2σ , $n = 4$) pg, with a ¹⁸⁷Os/¹⁸⁸Os ratio was 0.141 ± 0.052, making blank contributions of all analyzed samples less than 1% of the total Os measured.

Measurements of Re, Ru, Pd, Ir and Pt were made at UMD using a single collector, sector field, inductively coupled plasma mass spectrometer (Thermo Finnigan Element II) with an electron multiplier detector using an Aridus II micro flow nebulizer sample introduction system. The precision was better than 1% ($2\sigma_m$) for the ratio measurements of ¹⁸⁵Re/¹⁸⁷Re, ⁹⁹Ru/¹⁰¹Ru, ¹⁰⁵Pd/¹⁰⁶Pd, ¹⁹¹Ir/¹⁹³Ir and ¹⁹⁴Pt/¹⁹⁵Pt (100 cycles). Standard solutions of Ir and Ru (from Johnson-Matthey), Re, Pd and Pt (from the National Institute of Standards and Technology) were run before and after every four samples to correct for mass bias. The reference material TDB-1 yielded 0.074 ± 0.016 ng/g Ir, 0.212 ± 0.023 ng/g Ru, 5.0 ± 1.1 ng/g Pt, 22.0 ± 2.2 ng/g Pd and 1.05 ± 0.14 ng/g Re (2σ , $n = 5$), in good agreement with published results (Table 2). The results of two other reference materials (UB-N and OKUM) are also consistent with values reported in the literature (Table 2). The average total analytical blanks were 0.23 ± 0.13 pg Ir, 3.2 ± 2.7 pg

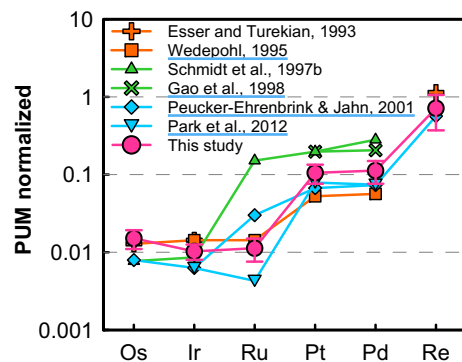


Fig. 1. Primitive upper mantle (PUM) normalized PGE and Re abundance estimates for the UCC from previous studies and this work. Primitive upper mantle values are from Becker et al. (2006) (here and elsewhere).

Ru, 62 ± 23 pg Pt, 7.0 ± 2.0 pg Pd and 1.78 ± 0.28 pg Re (2σ , $n = 4$). The blank contributions for all analyzed samples were less than 1.2% for Ir, 7.0% for Ru (excluding the Gaskiers composite, which is 13%), 8.1% for Pt (excluding the Konnarock composite, which is 14%), 1.2% for Pd and 5.4% for Re (excluding the Pocatello composite, which is 8.8%), and were corrected for all samples.

The analytical methods for total organic carbon (TOC) content can be found in Gaschnig et al. (2014). Briefly, about 5 g aliquots of powder were sequentially acidified with 3 M HCl for digesting carbonate and repeatedly washed with H₂O to get pH neutral solutions. Decalcified residues were dried down in an 80 °C oven and then homogenized. About 2–5 mg residues were weighed into tin cups for organic carbon determination with a Eurovector elemental analyzer. Contents measured were normalized to whole rock values according to the percent carbonate determined during acidification. The Cr and Ni concentrations were determined by solution ICP-MS using a high-pressure bomb dissolution method (original data, as well as completed methods, are reported in Gaschnig et al. (2016)). As some of the Mesoarchean diamictites are chromite-bearing, it was important to completely digest chromite to extract all Cr and PGEs. Because it is black, it was easy to see if chromite remained undigested. No chromite was observed following dissolution in our study, or in Gaschnig et al. (2016). Moreover, the much higher measured Cr and PGE concentrations relative to younger diamictites suggest complete dissolution of any original chromite.

4. RESULTS

4.1. Individual diamictite samples

To evaluate sample-to-sample heterogeneity within stratigraphic units, and to assess whether the compositions of the composites are representative of the units and/or time periods, three individual diamictite samples from each of the Mozaan, Gowganda, and Nantuo Formations and the two Bolivian formations were analyzed (Table A3 and

Table 2
PGE-Re concentrations and Os isotopes in reference materials.

References	Os ng/g	Ir ng/g	Ru ng/g	Pt ng/g	Pd ng/g	Re ng/g	¹⁸⁷ Os/ ¹⁸⁸ Os
<i>TDB-I, Diabase</i>							
This study, $n = 5$	0.146 ± 0.016	0.074 ± 0.016	0.212 ± 0.023	5.0 ± 1.1	22.0 ± 2.2	1.05 ± 0.14	0.94 ± 0.16
Peucker-Ehrenbrink et al. (2003), $n = 8$	0.122 ± 0.013	0.078 ± 0.012	4.40 ± 0.57	24.8 ± 1.8	0.832 ± 0.099		
Meisel and Moser (2004a,b), $n = 6$	0.117 ± 0.022	0.074 ± 0.020	0.199 ± 0.017	5.00 ± 0.39	24.4 ± 4.1	0.796 ± 0.049	0.92 ± 0.19
Ishikawa et al. (2014), $n = 32$	0.150 ± 0.070	0.077 ± 0.042	0.236 ± 0.092	4.8 ± 1.3	23.1 ± 3.8	0.99 ± 0.16	0.88 ± 0.33
<i>UB-N, Serpentinite</i>							
This study, $n = 1$	3.640	3.610	7.040	7.41	6.0	0.200	0.127
Puchtel et al. (2014), $n = 5$	3.79 ± 0.27	3.55 ± 0.32	6.88 ± 0.37	7.71 ± 0.07	6.10 ± 0.10	0.211 ± 0.010	0.12706 ± 16
Meisel and Moser (2004b), $n = 14$	3.85 ± 0.13	3.38 ± 0.22	6.30 ± 0.30	7.42 ± 0.30	6.11 ± 0.18	0.210 ± 0.004	
<i>OKUM, Komatiite</i>							
This study, $n = 1$	0.749	0.843	4.190	10.70	11.10	0.475	0.269
Savard et al. (2010)	0.790	0.943 ± 0.040	4.15 ± 0.08	11.44 ± 0.22	12.2 ± 0.73	0.566 ± 0.040	
Maier et al. (2012)	0.780	0.990	4.53	11.44	11.9		

Errors quoted at 2σ .

Fig. A1). The results show that, for a single formation and/or time period, PGE concentrations in the three individual samples are within the 50% deviation of their average, excluding Ru in the Gowganda Formation (69%), Pd in the Nantuo Formation (54%) and Os in the Bolivian formations (70%). In addition, concentrations of the four composites are within the concentration ranges of the corresponding three individual samples, respectively. However, the Re concentrations are highly variable, and potential reasons for this are discussed below. In general, the individual diamictite samples from one stratigraphic unit are relatively homogeneous in terms of PGE concentrations, and the PGE concentrations of the corresponding composites are representative of that of the stratigraphic units from which they derive.

4.2. Diamictite composites

Platinum-group element and Re concentrations, as well as Re–Os isotopic data for the 24 diamictite composites are provided in Table 3. As shown in Fig. 2, measured concentrations are double-normalized, with each analysis corrected for quartz, carbonate, or iron dilution by normalizing it to the average UCC Al_2O_3 content (15.4%; Rudnick and Gao, 2003), and then normalizing individual elements to estimates for primitive upper mantle (PUM, Becker et al., 2006). To obtain the common Os concentrations (Table 3), radiogenic ^{187}Os produced by ^{187}Re decay was subtracted, based on the depositional ages reported in the literature (Table A1) and the measured $^{187}\text{Re}/^{188}\text{Os}$. Due to the high solubility of Re, the measured $^{187}\text{Re}/^{188}\text{Os}$ may not represent the time-integrated $^{187}\text{Re}/^{188}\text{Os}$. Thus, the correction is not very precise, but has little impact on the conclusions. The radiogenic Os accounts for <30% of the measured Os concentrations, except for the Ramsay Lake (36%) and Gowganda (35%) composites.

The four Mesoarchean composites have similar Os, Ir, and Re abundances (Fig. 2a). However, the Afrikander composite is characterized by higher Ru, Pt, and Pd concentrations, compared to the Mozaan, Promise, and Coronation composites. The Afrikander composite also has higher first-row transition metal concentrations than the other three Archean composites (Fig. A2a), suggesting a greater fraction of chromite derived from mafic to ultramafic rocks. The high Cr (1132 $\mu\text{g/g}$) and Ru (1.89 ng/g) concentrations for the Afrikander composite are most likely caused by the presence of laurite-bearing chromites.

Among the seven Paleoproterozoic diamictite composites, the Duitschland composite has the highest PGE concentrations (Fig. 2b) and generally higher first-row transition metal contents (Fig. A2b), like the Afrikander composite, suggesting a greater contribution from ultramafic to mafic lithologies. The six remaining composites have roughly similar PUM-normalized PGE and Re patterns, which are systematically lower than those of Mesoarchean composites (Fig. 3).

The PGE and Re results for 10 Neoproterozoic composites (Fig. 2c) are characterized by similar PUM-normalized PGE patterns and generally similar first-row transition metal contents (Fig. A2c), but scattered Re. These compos-

ites have systematically lower PGE and Re concentrations than the older composites (Fig. 3).

Among the three Paleozoic composites (Fig. 2d), the Dwyka West composite, with the highest PGE concentrations, is similar to the Mesoarchean composites. Moreover, its first-row transition metal contents are between those of the Mesoarchean and Paleoproterozoic composites (Fig. A2d), and the age distribution of detrital zircons from this formation, at this locality, suggests that it is dominated by a pre-2.0 Ga provenance (Gaschnig et al., 2015). Accordingly, this composite is not included with the other Paleozoic composites in this study, both of which have similar PGE concentrations to the Neoproterozoic composites (Fig. 3).

The Re–Os isotopic systematics of the composites are provided in Table 2 and Fig. A3. The $^{187}\text{Os}/^{188}\text{Os}$ ratios are scattered, ranging from 0.2184 to 4.468. The $^{187}\text{Re}/^{188}\text{Os}$ ratios are highly variable, ranging between 1.28 and 813.

5. DISCUSSION

5.1. Sample representativeness

The idea of using glacial diamictites to estimate the average composition of the UCC originated with Goldschmidt (1933), who pointed out that the major-element contents obtained from glacial loams in Norway favorably corresponded to the averages of igneous -rock compositions. The ability of glaciers to sample wide areas of exposed crust are documented in studies of modern glacial tills from the Guys Bight Basin (Nesbitt and Young, 1996) and British Columbia (Canil and Lacourse, 2011), both of which show that such tills provide robust averages of the rocks that the glaciers traversed. The diamictites studied here represent lithified tills (e.g., Huber et al., 2001). Using the major and trace element concentrations of the diamictite composites investigated here, Gaschnig et al. (2016) demonstrated that they are good proxies not only for average elemental abundances of the present-day UCC, but also for tracking the compositional changes of the average UCC through time.

Below we discuss three important factors regarding the representativeness of the diamictites for average UCC PGE concentrations.

First, the ice sheets must sample sufficiently large areas of the continent so as to minimize the influence of local sources. Although the concentrations of some elements (e.g., Nb and Ta) in certain samples, like those comprising the Dwyka West and the Pocatello composites, are affected by local provenance (Gaschnig et al., 2016), other geochemical features are observed globally among samples of similar ages, implying that these signatures are representative of the exposed UCC (Gaschnig et al., 2014, 2016). For example, within a given time period the rare earth elements (REE) show similar concentrations and similar UCC-normalized patterns, with Al-normalized REE concentrations decreasing systematically from the Phanerozoic/Neoproterozoic, to the Paleoproterozoic, to the Archean (Fig. A4; Figs. 2 and 10 of Gaschnig et al., 2016). In a com-

Table 3
PGE concentrations and Re–Os isotopes of diamictite composites.

Sam. name	Os ^a	$2\sigma_m$ ^b	Os ^c	$2\sigma_m$	Ir	$2\sigma_m$	Ru	$2\sigma_m$	Pt	$2\sigma_m$	Pd	$2\sigma_m$	Re	$2\sigma_m$	$^{187}\text{Os}/^{188}\text{Os}$	$2\sigma_m$	$^{187}\text{Re}/^{188}\text{Os}$	Cr	Ni	Mo	TOC ^d
Mozaan	0.225	0.001	0.207	0.001	0.137	0.001	0.384	0.002	1.45	0.02	2.03	0.09	0.580	0.006	0.9317	0.0008	13.7	344	141	0.88	0.023
Mozaan*	0.208	0.001	0.190	0.001	0.115	0.001	0.394	0.002	1.85	0.03	2.09	0.10	0.575	0.006	0.9988	0.0007	14.8				
Afrikander	0.186	0.001	0.177	0.001	0.166	0.001	1.89	0.02	7.79	0.41	7.89	1.11	0.278	0.003	0.4548	0.0004	7.51	1132	227	0.47	0.025
Promise	0.315	0.001	0.301	0.001	0.203	0.002	0.635	0.005	1.55	0.02	1.78	0.06	0.448	0.004	0.4753	0.0004	7.15	386	152	0.77	0.053
Coronation	0.155	0.001	0.137	0.001	0.123	0.001	0.342	0.002	2.22	0.04	2.35	0.12	0.589	0.007	1.177	0.001	20.7	294	114	3.0	0.046
Duitschland	0.265	0.002	0.263	0.002	0.194	0.002	0.308	0.002	10.9	0.8	12.2	2.7	0.0791	0.0007	0.2184	0.0003	1.45	164	61.3	0.55	0.130
Timeball Hill	0.0643	0.0001	0.0486	0.0002	0.0399	0.0003	0.0922	0.0005	0.964	0.009	0.993	0.026	0.659	0.006	2.851	0.002	66.9	123	38.7	1.3	0.183
Makganyene	0.236	0.001	0.191	0.001	0.0412	0.0003	0.0881	0.0005	0.781	0.007	0.894	0.025	1.81	0.03	1.921	0.001	45.6	82.4	37.3	1.0	0.174
Ramsay Lake	0.0737	0.0001	0.0537	0.0003	0.0565	0.0003	0.0736	0.0006	2.24	0.04	2.77	0.18	0.786	0.009	4.468	0.002	80.4	74.7	39.7	2.3	0.035
Bruce	0.0699	0.0001	0.0526	0.0002	0.0448	0.0003	0.0931	0.0005	1.20	0.01	1.11	0.03	0.680	0.007	3.348	0.002	66.5	111	32.4	1.5	0.039
Gowganda	0.0583	0.0001	0.0466	0.0001	0.0462	0.0003	0.100	0.001	1.33	0.02	1.49	0.05	0.477	0.004	2.723	0.002	52.8	121	55.9	1.8	0.033
Bottle Creek	0.0338	0.0001	0.0331	0.0001	0.0318	0.0002	0.0676	0.0005	0.719	0.007	0.499	0.008	0.0268	0.0003	2.409	0.002	4.95	96.2	37.8	0.58	0.045
Gaskiers	0.0121	0.0001	0.0116	0.0001	0.0066	0.0001	0.0080	0.0002	0.276	0.002	0.241	0.002	0.0798	0.0007	0.7083	0.0008	34.1	64.2	25.9	1.2	0.035
Pocatello*	0.0146	0.0001	0.0146	0.0001	0.0141	0.0001	0.0278	0.0002	0.329	0.004	0.224	0.003	0.0068	0.0001	1.597	0.002	2.66	44.7	21.9	0.48	0.034
Pocatello*	0.0153	0.0001	0.0152	0.0001	0.0187	0.0002	0.0305	0.0004	0.364	0.005	0.220	0.002	0.0068	0.0001	1.494	0.001	2.51				
Konnarock	0.0403	0.0004	0.0402	0.0004	0.0084	0.0001	0.0154	0.0001	0.145	0.002	0.169	0.002	0.0110	0.0001	0.4229	0.0020	1.37	25.6	11.4	0.56	0.050
Nantuo	0.0358	0.0001	0.0352	0.0001	0.0264	0.0002	0.0236	0.0002	0.637	0.015	0.402	0.013	0.0877	0.0004	0.7528	0.0007	12.8	55.7	28.8	0.32	0.080
Gucheng	0.0205	0.0001	0.0199	0.0001	0.0229	0.0002	0.0268	0.0002	0.566	0.009	0.453	0.007	0.0851	0.0004	0.9602	0.0011	22.2	66.0	34.9	0.33	0.150
Blaubeker	0.0549	0.0001	0.0548	0.0001	0.0263	0.0003	0.0417	0.0004	0.586	0.011	0.468	0.008	0.0124	0.0001	1.498	0.001	1.28	39.0	14.1	0.49	0.029
Kaigas	0.132	0.002	0.129	0.002	0.0216	0.0002	0.0336	0.0003	0.553	0.010	0.305	0.004	0.316	0.002	1.500	0.004	13.6	58.9	29.5	1.0	0.063
Chuos	0.0611	0.0002	0.0603	0.0002	0.0336	0.0003	0.0452	0.0003	0.526	0.005	0.576	0.010	0.112	0.001	0.9860	0.0012	9.8	31.0	29.5	0.61	0.111
Numees	0.0162	0.0001	0.0157	0.0001	0.0094	0.0001	0.0192	0.0002	0.257	0.003	0.364	0.006	0.0742	0.0005	3.359	0.005	31.3	29.0	16.0	0.43	0.093
Ghaub	0.0537	0.0002	0.0533	0.0002	0.0245	0.0002	0.0384	0.0003	0.341	0.003	0.323	0.005	0.0516	0.0003	1.143	0.002	5.24	44.9	17.4	0.46	0.090
Bolivian	0.0290	0.0001	0.0171	0.0002	0.0179	0.0002	0.0285	0.0003	0.328	0.004	0.206	0.004	3.43	0.06	3.381	0.003	813	50.0	18.4	0.24	0.250
Dwyka West	0.132	0.001	0.120	0.001	0.0939	0.0007	0.399	0.004	2.74	0.10	2.46	0.10	3.68	0.04	1.825	0.002	165	164	79.9	2.9	0.369
Dwyka East	0.0442	0.0002	0.0421	0.0002	0.0336	0.0003	0.0867	0.0011	0.963	0.021	0.931	0.018	0.665	0.003	1.381	0.002	84.2	95.4	32.5	0.73	0.190

The concentration unit for PGEs and Re is ng/g and for Cr, Ni and Mo is $\mu\text{g/g}$.

The Cr, Ni and Mo data are from [Gaschnig et al. \(2016\)](#).

^a Measured Os concentrations.

^b The σ_m (standard deviation of the mean) was obtained by error propagation from the σ_m of measured isotopic ratios (100 cycles).

^c Os concentrations with radiogenic Os removed (common Os).

^d Total organic carbon (wt%).

* Replicate.

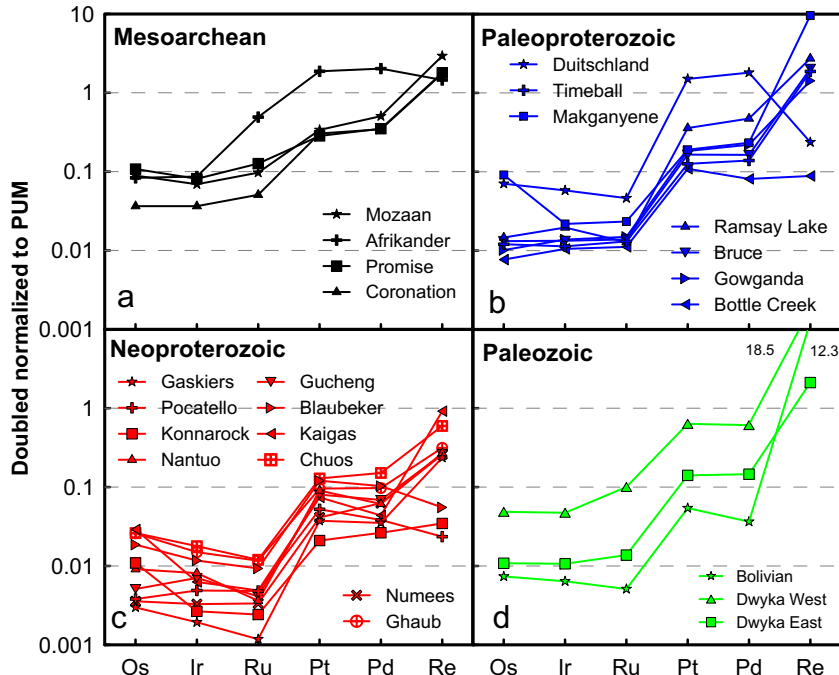


Fig. 2. Doubled normalized PGE and Re concentrations of all 24 diamictite composites grouped by depositional ages. Measured concentrations are double-normalized, with each analysis corrected for quartz dilution by normalizing it to the average UCC_{R&G} Al₂O₃ content (15.4%; Rudnick and Gao, 2003), and then normalizing individual elements to PUM. Osmium concentrations have been corrected for radiogenic ingrowth of ¹⁸⁷Os from ¹⁸⁷Re decay.

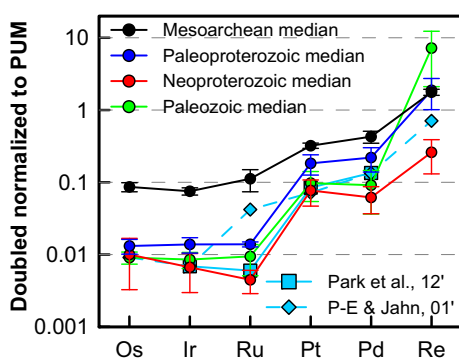


Fig. 3. Doubled normalized median PGE and Re concentrations of diamictite composites from each time interval. Osmium concentrations for diamictite composites have been corrected for radiogenic ingrowth of ¹⁸⁷Os from ¹⁸⁷Re decay. Errors quoted at MAD (median absolute deviation).

plementary fashion, the insoluble first-row transition element concentrations increase systematically from the Phanerozoic/Neoproterozoic, to the Paleoproterozoic, to the Archean (Fig. A2; Fig. 3 of Gaschnig et al., 2016). Both features reflect a greater proportion of mafic/ultramafic rocks in the Archean crust, as has been previously documented (Taylor and McLennan, 1985; Condie, 1993; Keller and Schoene, 2012; Tang et al., 2016). The glacial diamictites thus appear to be sampling large continental areas.

A second concern is whether the samples derive from a wide enough geographic region to represent a global average. While the diamictites from the three younger periods were sampled from different continents that were geographically dispersed at the time of deposition (Gaschnig et al., 2014), the Mesoarchean diamictites are all from two adjacent Archean sedimentary basins in South Africa, the Afrikander, Promise and Coronation Formations from the Witwatersrand Basin, and the Mozaan Formation from the Pongola Basin. Unfortunately, the incomplete nature of the geologic record leaves no better approach for studying the average composition of the Archean UCC through diamictites, as these are the only such samples of which we are aware. Moreover, there are no loess deposits of appropriate ages, and other fine-grained sediments (e.g., shale, mudstone) are the products of chemical weathering, which preferentially removes more soluble elements. The similarity in REE patterns (Fig. A5) and insoluble transition metals (Fig. 3 of Tang et al., 2016) between Archean diamictites and Archean shales suggest that the diamictites, like the shales, provide a representative sample of the Archean UCC. Several previous studies have suggested that some diamictites could be produced by catastrophic impact events (e.g., Oberbeck et al., 1993; Koeberl and Montanari, 2000), which may elevate the PGE concentrations of the diamictites, leading to higher PGE concentrations in the Mesoarchean diamictite composites. However, based on petrographic and geochemical evidence, Huber et al. (2001) concluded that neither geochemical nor petrographic

evidence supports an impact origin of the diamictites from the Witwatersrand Supergroup in South Africa.

Third, the composition of the diamictites should not be modified by syn- or post-depositional processes, such as density sorting and chemical weathering. The PGEs are mainly hosted in platinum group minerals that have densities up to 10 times higher than silicates (in the case of Os–Ir nuggets). Thus, transportation by wind may create a severe segregation of PGEs within these sediments. Such density sorting has impacted loess compositions, which show anomalously high concentrations of zirconium ($477 \pm 135 \mu\text{g/g}$, 1σ , [Taylor et al., 1983](#); [Barth et al., 2000](#)), which has been attributed to the eolian concentration of zircon. By contrast, the zirconium concentrations in diamictites ($188 \pm 99 \mu\text{g/g}$, 1σ) are similar to the average UCC Zr abundance ($193 \pm 28 \mu\text{g/g}$, 1σ , [Rudnick and Gao, 2003](#)), and are much lower than in loess ([Taylor et al., 1983](#); [Barth et al., 2000](#)). Moreover, there is no evidence for wind sorting in the diamictites, which are, by definition, extremely poorly sorted. Consequently, unlike loess, wind sorting is unlikely to affect the composition of the glacial diamictites.

By contrast, nearly all of the diamictites record a weathering signature in their chemical compositions ([Gaschnig et al., 2014, 2016; Li et al., 2016](#)). For example, the chemical index of alteration (CIA = molar $\text{Al}_2\text{O}_3/(\text{K}_2\text{O} + \text{Na}_2\text{O} + \text{CaO}^*)$, where CaO^* is CaO associated with the silicate fraction of the bulk sample) for most of the diamictites is high (~55 to ~75), above those of igneous rocks (<55) ([Gaschnig et al., 2016](#)). Using Li and Pb isotopes, [Li et al. \(2016\)](#) showed that the intensity of the weathering signature in the diamictites increases as one goes back in time and concluded that the weathering signature is largely inherited from the provenance of the diamictites; there has been very limited post- or syn-depositional chemical weathering. This inference is supported by correlations between PGE and insoluble transition elements, described in Section 5.2.1, below (see also Figs. 4, A6 and A7), which imply little post- or syn-depositional modification of the PGE concentrations. If so, then the diamictites should

provide a faithful record of the average UCC composition, including any weathered regolith that existed at the surface.

5.2. Present-day UCC PGE abundances and Re–Os isotopes

There are two ways to estimate the chemical composition of the present-day average UCC using fine-grained sedimentary rocks. One way is to adopt the median or average elemental concentrations in fine-grained terrigenous sedimentary rocks to represent the average UCC composition. This method can only be applied to insoluble elements (e.g., Th, Fe, Al and REE) that are not fractionated or affected during sedimentary processing ([Taylor and McLennan, 1985](#); [Rudnick and Gao, 2003](#); [Gaschnig et al., 2016](#)). In order to obtain a good estimate (e.g., small uncertainty), a large number of samples from different areas are generally needed. The other approach is to use the correlation between an element of interest and another element whose concentration is well constrained in the UCC (e.g., La) ([Taylor and McLennan, 1985](#); [McLennan, 2001](#); [Rudnick and Gao, 2003](#); [Hu and Gao, 2008](#); [Gaschnig et al., 2016](#)). Below we explore the utility of both approaches in estimating the average PGE and Re concentrations of the present-day UCC.

5.2.1. PGE abundances: median approach

In order to use this method, the mobility of the PGEs during chemical weathering and any chemical fractionation associated with physical weathering, sediment transport and sorting, as well as diagenesis, must be evaluated. Such influences may differ from element to element. Of the limited work that has been done to constrain PGE solubility, Os appears to be moderately soluble during oxidative weathering ([Peucker-Ehrenbrink and Blum, 1998](#); [Peucker-Ehrenbrink and Hannigan, 2000](#); [Jaffe et al., 2002](#)). Based on a study of fresh and weathered black shales, [Peucker-Ehrenbrink and Hannigan \(2000\)](#) concluded that Ir, Pt and Pd were also moderately soluble, whereas [Jaffe et al. \(2002\)](#) inferred from a weathering profile through black shale that the three elements were essentially

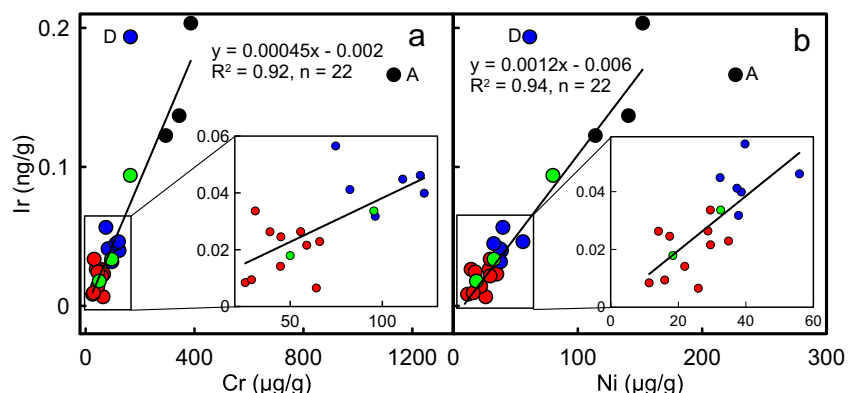


Fig. 4. Correlations between Ir and Cr (a), Ni (b) for diamictite composites from this study. Black, blue, red and green circles denote Mesoarchean, Paleoproterozoic, Neoproterozoic and Paleozoic diamictite composites, respectively. Symbols with letters near them (D: Duitschland; A: Afrikander) are not incorporated in the regression calculations. The “n” is the sample numbers used in the regression calculation. Equations are obtained using a bootstrapping resample method (see Section 5.2.2). (For interpretation of the references to color in this figure legend, the reader is referred to the web version of this article.)

insoluble. By contrast, it is well established that Re is highly soluble in the near-surface, oxidized environment (Colodner et al., 1993; Peucker-Ehrenbrink and Hannigan, 2000; Jaffe et al., 2002). Therefore, PGEs tend to stay in the solid phase during chemical weathering and their concentrations in diamictites most likely represent their abundances in the UCC, but the same is not true for Re.

Here we compare inter-element correlations between PGEs and insoluble transition metals (e.g., Cr, Ni; Taylor and McLennan, 1985) with those between PGEs and soluble transition metals (e.g., Re, Mo; Taylor and McLennan, 1985) to infer the relative solubility of the PGEs during the formation of the diamictites. If the PGEs show significant positive correlations with insoluble transition metals, but no correlations with soluble transition metals, they were likely insoluble. In Figs. 4, A6 and A7, strong positive correlations of Ir, Ru, Pt, Pd versus Cr and Ni ($R^2 \geq 0.70$) and fair correlations of Os versus Cr and Ni ($R^2 = 0.58$) are observed for the diamictite composites. No correlations, however, are observed between the PGEs and Re or Mo (not shown). Therefore, Ir, Ru, Pt and Pd are presumed to be insoluble, and Os is likely moderately insoluble, during the formation of these diamictites.

We use the median PGE concentrations of the post-Paleoproterozoic diamictite composites, which is less affected by extremely high or low values than average values, in order to estimate their abundances in the present-day UCC. The same method has been used by Gaschnig et al. (2016) to infer the major and trace element abundances in the present-day UCC from the post-Paleoproterozoic diamictites. Many studies, based on both sedimentary and igneous rocks, have demonstrated that the UCC composition changed at the Archean–Proterozoic boundary, after which no obvious change in composition is observed (Taylor and McLennan, 1985; Condie, 1993; Taylor and McLennan, 2008; Keller and Schoene, 2012; Tang et al., 2016). This is why Taylor and McLennan (1985) used post-Archean shales to estimate the REE abundances in the modern UCC. Since our Paleoproterozoic diamictites (~2.2–2.5 Ga) contain a higher proportion of Archean UCC rocks than the younger diamictites, we still see compositional changes between Paleoproterozoic and Neoproterozoic diamictites (e.g., REE and first-row transition metals). Therefore, we excluded both Archean and Paleoproterozoic diamictites when applying the median method. The Dwyka West composite (Paleozoic) was not incorporated here because its provenance is Archean crust (Gaschnig et al., 2015). The median values and the median absolute deviation (MAD, defined as the median of the absolute deviations of the measurements from the population median) are listed in Table 4. The average values of the post-Paleoproterozoic diamictite composites, which are not shown here, are similar to the medians.

5.2.2. PGE abundances: regression approach

The least-squares regression approach has been widely used to estimate trace element abundances in the UCC (McLennan, 2001; Rudnick and Gao, 2003; Hu and Gao, 2008) by calculating the slope and intercept of the

Table 4
Average PGE abundance estimates (ng/g) in the UCC of various time periods.

	Mesoarchean UCC		Paleoproterozoic UCC		Neoproterozoic UCC		Phanerozoic UCC		Present-day UCC	
	Mesoarchean composites, $n = 4^a$	Model calculation ^b	Paleoproterozoic composites, $n = 7^a$		Neoproterozoic composites, $n = 10^a$		Model calculation ^b		Median approach ^c	Regression approach ^d
			Phanerozoic	composites, $n = 2^a$	Phanerozoic	composites, $n = 2^a$				
Os	0.192 ± 0.035 ^e		0.053 ± 0.006 ^e		0.038 ± 0.020 ^e		0.030 ± 0.013 ^e		0.038 ± 0.017	0.059 ± 0.016
Ir	0.152 ± 0.022		0.08–0.16	0.045 ± 0.005	0.022 ± 0.006		0.026 ± 0.008		0.022 ± 0.006	0.036 ± 0.008
Ru	0.51 ± 0.15		0.21–0.46	0.092 ± 0.007	0.027 ± 0.010		0.059 ± 0.029		0.028 ± 0.010	0.079 ± 0.026
Pt	1.89 ± 0.39		1.8–2.9	1.20 ± 0.42	0.43 ± 0.14		0.65 ± 0.32		0.43 ± 0.14	0.80 ± 0.22
Pd	2.19 ± 0.29		1.8–2.7	1.11 ± 0.38	0.34 ± 0.11		0.57 ± 0.36		0.76	0.82 ± 0.26

^a For each time period, the median values (consistent with averages) from diamictites are taken as the average PGE abundances for the UCC in that period. The errors quoted at MAD (median absolute deviation).

^b Calculated using the average PGE concentrations of rocks in Table A5 and the relative proportions of rock types in Condie's (1993) restoration model and the model from Tang et al. (2016) in Table A6. No PGE data for felsic rocks are published and their PGE concentrations are assumed to be zero. The PGE abundances in the Proterozoic UCC are not provided here as few data have been reported for Proterozoic rocks.

^c Obtained from the “Median approach”, see Section 5.2.1. Errors quoted at MAD.

^d Obtained from the “Regression approach”, see Section 5.2.2.

^e The Os concentrations used for medians are common Os.

regression, and then the projected element concentration of interest. However, the uncertainty of the projected concentration cannot be obtained by this method when the uncertainty of the regression itself is considered. Thus, to calculate the uncertainty on the projected concentration of the element of interest, we used a bootstrapping resampling method (Efron and Tibshirani, 1993; see Appendix “how bootstrapping works”). For example, for the Cr–Ir correlation (Fig. 4a), we first randomly resampled the Cr–Ir dataset ($n = 22$), allowing a single point to be sampled more than once. The size of each resample is equal to that of the original Cr–Ir dataset ($n = 22$). For each resample, we calculated a slope and an intercept using the least-squares regression, and a projected Ir concentration at the average upper crustal Cr abundance of $82 \pm 16 \text{ }\mu\text{g/g}$ ($2\sigma_m$) (see next section for derivation of this value). The uncertainties on the Cr and Ir concentrations for each composite and the recommended UCC Cr abundance are all taken into account. We repeated this step 10,000 times to get 10,000 resamples, which gives us 10,000 regressions and 10,000 projected Ir concentrations, respectively. We took the final average Ir concentration of the 10,000 projected Ir concentrations and the standard deviation as the UCC Ir abundance and associated precision, respectively. Below we perform the regressions using the composites from all four time periods ($n = 24$, unless otherwise indicated), as the modern UCC contains rocks with ages ranging from $\sim 4.0 \text{ Ga}$ to $\sim 0 \text{ Ma}$ and all the UCC rocks contribute to the composition of the modern UCC. Regressions were also performed using a subset that excluded the four Mesoarchean samples (results not shown here). The resulting PGE abundance estimates were found to be identical, within uncertainty, with those obtained from the entire data set, which supports the idea that samples with all ages should be incorporated into the regression.

As shown in Fig. 4, Ir is strongly positively correlated with Cr ($R^2 = 0.92$) and Ni ($R^2 = 0.94$). The averages of published UCC abundance estimates for Cr ($82 \pm 16 \text{ }\mu\text{g/g}$, $2\sigma_m$, $n = 6$) and Ni ($42 \pm 10 \text{ }\mu\text{g/g}$, $2\sigma_m$, $n = 6$) (Condie, 1993; Gao et al., 1998; McLennan, 2001; Rudnick and Gao, 2003; Hu and Gao, 2008; Gaschnig et al., 2016) are taken as their UCC abundances. The Ir concentrations obtained from the above two regressions are within uncertainty of one another, with values of 0.036 ± 0.008 and $0.044 \pm 0.012 \text{ ng/g}$ (2σ), respectively. Considering the lower relative standard deviation, we adopt $0.036 \pm 0.008 \text{ ng/g}$ as the Ir abundance estimate of the UCC. Our Ir abundance is higher by 60–80% than the two prior estimates based on data from loess (Peucker-Ehrenbrink and Jahn, 2001; Park et al., 2012), and the surface sampling-based estimate (Shaw et al., 1976) (Table 1, Fig. 1). It is lower by $\sim 40\%$ than the estimates of Esser and Turekian (1993) and Wedepohl (1995), based upon river sediments and greywackes, respectively, and is similar to the value reported by Schmidt et al. (1997a), based upon impact melt rocks (Table 1, Fig. 1).

Common Os shows a strong positive correlation with Ir ($R^2 = 0.89$, Fig. 5a), and fair correlations with Cr ($R^2 = 0.58$) and Ni ($R^2 = 0.58$) (Fig. A6a and b), respectively. Using the above Ir concentration estimate, the good

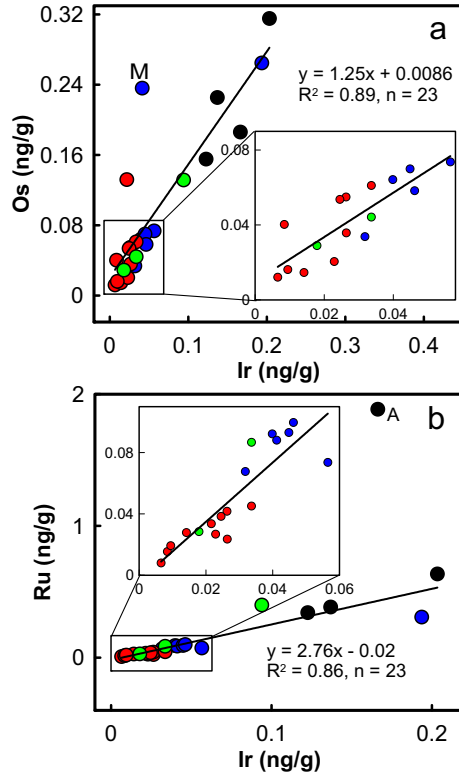


Fig. 5. Correlations between Ir and Os (a), Ru (b) for diamictite composites from this study. The Os concentrations plotted for diamictite composites are common Os (Table 2). Symbols with letters near them (M: Makganyene; A: Afrikander) are not incorporated in the regression calculation. The “ n ” is the sample numbers used in the regression calculation. See Fig. 4 for symbols.

correlation between Ir and Os leads to an Os abundance of $0.054 \pm 0.016 \text{ ng/g}$ (2σ). This Os value is within uncertainties of those obtained from the other two regressions, which give concentrations of 0.066 ± 0.024 and $0.077 \pm 0.028 \text{ ng/g}$ (2σ) using the above UCC Cr and Ni estimates, respectively. Since Os correlates best with Ir and the Os–Ir correlation yields a lower relative standard deviation, the concentration of $0.054 \pm 0.016 \text{ ng/g}$ obtained from the Ir–Os regression is taken as the average common Os abundance for the UCC. Adding radiogenic Os back to common Os using the Re abundance of $0.25 \pm 0.12 \text{ ng/g}$ (Section 5.2.3), an Os abundance of $0.059 \pm 0.016 \text{ ng/g}$ (2σ) is obtained (Table 4). Our Os estimate is within uncertainty of those obtained by Esser and Turekian (1993), but is about twice as high as those of Schmidt et al. (1997a) and Peucker-Ehrenbrink and Jahn (2001) (Table 1, Fig. 1).

Figs. 5b and A6c and d illustrate the good correlations observed between Ru and Ir ($R^2 = 0.86$), Cr ($R^2 = 0.98$) and Ni ($R^2 = 0.88$), respectively. These regressions yield Ru concentrations of 0.079 ± 0.026 , 0.082 ± 0.034 and $0.112 \pm 0.046 \text{ ng/g}$ (2σ), respectively. In view of the lower relative standard deviation of the result obtained from the Ir–Ru regression, the concentration obtained from this correlation ($0.079 \pm 0.026 \text{ ng/g}$) is adopted as our Ru concentration estimate for the UCC. Previous Ru abundance estimates for the UCC varied by nearly two orders of

magnitude (0.03–1.06 ng/g, Table 1, Fig. 1) (Wedepohl, 1995; Schmidt et al., 1997a; Peucker-Ehrenbrink and Jahn, 2001; Park et al., 2012). The highest Ru abundance estimate of 1.06 ng/g (Table A5) was obtained from impact melt samples by Schmidt et al. (1997a), using NiS fire assay combined with neutron activation. The reason for the unexpected high Ru estimate remains unclear. Peucker-Ehrenbrink and Jahn (2001) estimated an abundance of 0.210 ng/g. This Ru estimate is nearly an order of magnitude higher than the estimate of 0.0030 ng/g reported by Park et al. (2012). Park et al. (2012) suggested the higher Ru concentrations reported by Peucker-Ehrenbrink and Jahn (2001) may have resulted from an analytical artifact. Our Ru estimate of 0.079 ng/g falls between the estimates of Park et al. (2012) and Wedepohl (1995) (0.1 ng/g, Table 1, Fig. 1).

As shown in Figs. 6a and A7a and b, Pt is strongly positively correlated with Ru ($R^2 = 0.89$), Cr ($R^2 = 0.87$) and Ni ($R^2 = 0.70$). These correlations yield similar Pt concentrations of 0.80 ± 0.22 , 0.80 ± 0.26 and 0.95 ± 0.34 ng/g (2σ), respectively. In light of the lower relative standard deviation of the result obtained from the Ru–Pt regression correlation, 0.80 ± 0.22 ng/g is taken as the Pt UCC abundance estimate. Palladium shows an excellent correlation with Pt ($R^2 = 0.99$) (Fig. 6b), and good correlations with Cr ($R^2 = 0.87$) and Ni ($R^2 = 0.74$) (Fig. A7c and d), yielding similar Pd concentrations of 0.80 ± 0.26 , 0.80 ± 0.28 and 0.96 ± 0.36 ng/g (2σ), respectively. Here, we use 0.80 ± 0.26 ng/g as the Pd abundance for the UCC because of the lower relative standard deviation. Because Ir, Ru, Pt and Pd become progressively more incompatible in many silicate systems from Ir to Pd (e.g., Pearson et al., 2004), correlations between Ru and Pt are better than Ir–Pt, and Pt–Pd is better than Ir–Pd. Although the Pt and Pd abundance estimates obtained from Ir–Pt and Ir–Pd correlations are within uncertainties of those from Ru–Pt and Pt–Pd correlations, the latter yield lower uncertainties. This is why here we use Ru–Pt and Pt–Pd correlations, instead of Ir–Pt and Ir–Pd correlations. The Pt and Pd concentrations obtained by Gao et al. (1998) and Schmidt et al. (1997a), are generally three times higher than those derived from sedimentary averages (Table 1, Fig. 1) (Wedepohl, 1995;

Peucker-Ehrenbrink and Jahn, 2001; Park et al., 2012).

Our Pt and Pd estimates lie between these two types of estimates (Table 1, Fig. 1). In contrast to the differences in absolute concentrations, all of the previous Pd/Pt ratio estimates, as well as the one from this study, are similar, ranging from 0.88 to 1.02 (with a slightly higher ratio of 1.33 from Schmidt et al., 1997a). This suggests that these two elements are not fractionated during weathering and sediment transport, and have similar abundances in the UCC.

5.2.3. Re–Os isotopes

Rhenium is highly soluble in the near-surface, oxidized environment (Colodner et al., 1993; Peucker-Ehrenbrink and Hannigan, 2000; Jaffe et al., 2002), as is reflected in the weak correlation between Re and the soluble element Mo (Fig. 7b). This results in highly variable Re concentrations in different types of sedimentary samples, and a general lack of correlation between Re and other trace elements. Estimating the UCC Re abundance and $^{187}\text{Re}/^{188}\text{Os}$ ratio is, thus, challenging. Esser and Turekian (1993) used Fe–Ir–Os correlations in river sediments to estimate the UCC Os abundance. Then they used sample $^{187}\text{Os}/^{188}\text{Os}$ ratios and associated Nd model ages to calculate a time-integrated $^{187}\text{Re}/^{188}\text{Os}$ ratio for each sample, assuming that Os has the same crustal residence age as Nd. The average of the obtained $^{187}\text{Re}/^{188}\text{Os}$ ratios of all samples was taken as the present-day UCC $^{187}\text{Re}/^{188}\text{Os}$ ratio. Thus, the present-day UCC $^{187}\text{Os}/^{188}\text{Os}$ ratio and Re concentration can be recalculated using the above average $^{187}\text{Re}/^{188}\text{Os}$ ratio and the average Nd model age for the North American basement (~2.2 Ga, Esser and Turekian, 1993). A similar approach was applied to loess samples from China by Peucker-Ehrenbrink and Jahn (2001).

This method, however, cannot be applied to all of the diamictite composites, because they are characterized by much more variable $^{187}\text{Os}/^{188}\text{Os}$ ratios than river sediments and loess samples (Fig. A3). Therefore, contrary to the two previous studies (Esser and Turekian, 1993; Peucker-Ehrenbrink and Jahn, 2001) in which the UCC Os abundance and $^{187}\text{Re}/^{188}\text{Os}$ ratio were first estimated, and then the UCC $^{187}\text{Os}/^{188}\text{Os}$ ratio and Re abundance were calculated, here we first estimate the UCC Os and Re abun-

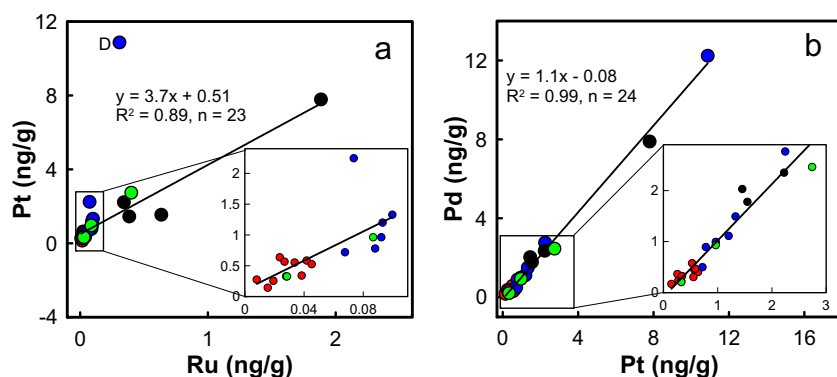


Fig. 6. Correlations between Pt and Ru (a), and between Pd and Pt (b). Symbols with letters near them (D: Duitschland) are not incorporated in the regression calculations. The “n” is the sample numbers used in the regression calculation. See Fig. 4 for symbols.

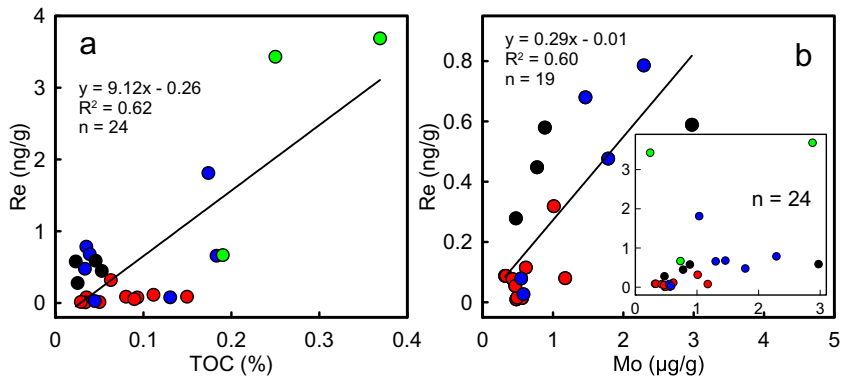


Fig. 7. Correlations between Re and TOC (a) and between Re and Mo (b) in diamictite composites. Five composites (Timeball Hill, Makganyene, Bolivian, Dwyka West and Dwyka East) with relatively high TOC contents and Re concentrations are not used in the Re–Mo regression calculation and are shown in the inset. See Fig. 4 for symbols.

dances using the regression approach. We then calculate the UCC $^{187}\text{Re}/^{188}\text{Os}$ ratio and finally obtain the UCC $^{187}\text{Os}/^{188}\text{Os}$ ratio.

The geochemical behavior of Re is generally similar to that of Mo. In oxidizing aqueous environments, Re and Mo are oxidized to ReO_4^- and MoO_4^{2-} , which are highly soluble, and thus enriched in seawater relative to UCC rocks (Ravizza et al., 1991; Anbar et al., 1992; Colodner et al., 1993). Under sulfidic conditions, both elements can be enriched in marine sediments (Crusius et al., 1996; Morford and Emerson, 1999). The difference is that Re, but not Mo, can also be enriched in sediments under suboxic conditions (Crusius et al., 1996; Morford and Emerson, 1999; Miller et al., 2011), suggesting that Re is scavenged more readily than Mo. This difference is reflected in the diamictites, which generally show a weathering signature inherited from their provenance (Li et al., 2016). A weak correlation between Re and total organic carbon (TOC) is observed in the diamictite composites (Fig. 7a), whereas there is no correlation between Mo and TOC (not shown). The organic carbon contents in these diamictite composites are relatively low (<0.4%), and the observed correlations (or lack thereof) suggests limited Mo scavenging, but some Re scavenging. Excluding the five diamictites with the highest TOC in order to eliminate samples that experienced Re scavenging, we find a weak correlation between Re and Mo in the diamictite composites (Fig. 7b).

From this correlation, an UCC Re abundance of $0.25 \pm 0.12 \text{ ng/g}$ (2σ) can be obtained by the bootstrapping resample method, using the average of UCC Mo estimates ($0.9 \pm 0.3 \mu\text{g/g}$, $2\sigma_m$, $n = 6$) from the literature (Sims et al., 1990; Wedepohl, 1995; Gao et al., 1998; Rudnick and Gao, 2003; Hu and Gao, 2008; Gaschnig et al., 2016). The relatively large standard deviation on this estimate is caused by the large uncertainty of the UCC Mo abundance and the weak correlation between Re and Mo. Additionally, the Re concentrations in igneous rocks are significantly lower (up to three to four orders of magnitude) than those of organic-rich sediments (Dubin and Peucker-Ehrenbrink, 2015). The extreme heterogeneity of Re concentrations in UCC rocks and the disproportionate influence of heteroge-

neously distributed organic-rich sediments on the UCC average (Dubin and Peucker-Ehrenbrink, 2015) also provide challenges in estimating UCC Re abundance with a relatively small uncertainty. Our estimate lies between the estimates reported by the two previous studies (Table 1, Fig. 1, Esser and Turekian, 1993; Peucker-Ehrenbrink and Jahn, 2001).

Using the new Re and Os estimates from this work, the $^{187}\text{Re}/^{188}\text{Os}$ ratio of the UCC is calculated to be 20 ± 12 (2σ) (Table 1). Assuming an average age of the UCC of $\sim 2.0 \text{ Ga}$ (Allègre and Rousseau, 1984), the present-day $^{187}\text{Os}/^{188}\text{Os}$ ratio of the UCC is 0.80 ± 0.38 (2σ). Our lower estimates of $^{187}\text{Re}/^{188}\text{Os}$ and $^{187}\text{Os}/^{188}\text{Os}$ ratios than the previous studies (Esser and Turekian, 1993; Peucker-Ehrenbrink and Jahn, 2001; Dubin and Peucker-Ehrenbrink, 2015) are mainly caused by our higher UCC Os abundance estimate (Table 1). The large uncertainty of our estimated $^{187}\text{Re}/^{188}\text{Os}$ and $^{187}\text{Os}/^{188}\text{Os}$ ratios mainly result from the large uncertainty of the estimated Re concentration.

Another way to estimate the $^{187}\text{Os}/^{188}\text{Os}$ ratio of the present-day UCC is, similar to the “Median approach”, to use the median value of the Neoproterozoic and Paleozoic composites (again excluding the Dwyka West composite for the reasons stated above), yielding a result of 1.26 ± 0.32 ($n = 12$, MAD). This ratio is consistent, within uncertainty, with the average $^{187}\text{Os}/^{188}\text{Os}$ ratio of the Neoproterozoic and Paleozoic composites, which is 1.47 ± 0.61 ($n = 12$, 95% confidence interval). Both estimates are slightly higher, but within uncertainty of the ratio (0.80 ± 0.38 (2σ)) calculated from the UCC Re and Os abundances. Considering that the sample $^{187}\text{Os}/^{188}\text{Os}$ ratio can be readily affected by the concentration of Re, which is a highly soluble element and shows scattered concentrations in diamictite composites (from 0.0068 to 3.68 ppb), and the $^{187}\text{Os}/^{188}\text{Os}$ ratios of the Neoproterozoic and Paleozoic composites are still variable (from 0.4229 to 3.381), the median or average $^{187}\text{Os}/^{188}\text{Os}$ ratio may not be representative of the average UCC. Here we take 0.80 ± 0.38 (2σ) and 20 ± 12 (2σ) as our best estimate of $^{187}\text{Os}/^{188}\text{Os}$ and $^{187}\text{Re}/^{188}\text{Os}$ ratios of the present-day UCC.

5.3. The role of old crust in the present-day UCC

Both loess and diamictite have been used as proxies for the composition of the UCC (Taylor et al., 1983; Gallet et al., 1998; Jahn et al., 2001; McLennan, 2001; Peucker-Ehrenbrink and Jahn, 2001; Rudnick and Gao, 2003; Hu and Gao, 2008; Park et al., 2012; Gaschnig et al., 2016). Our present-day UCC PGE abundance estimates from the medians or averages of post-Paleoproterozoic composites are similar to those obtained from loess samples, (Tables 1 and 4, Peucker-Ehrenbrink and Jahn, 2001; Park et al., 2012). These estimates are systematically lower than those obtained by the regression approach using all diamictite composites in this study (Table 4). We suggest the reason for the difference is that loess and our Neoproterozoic and Paleozoic diamictites preferentially sample younger UCC rocks, which have lower PGE, Cr and Ni concentrations than older crust, as reflected in shales (Taylor and McLennan, 1985; Condie, 1993), large scale surface averages (Eade and Fahrig, 1973; Condie, 1993), and data compilation (Keller and Schoene, 2012). This is supported by the fact that loess samples generally have Nd model ages of $\sim 1.0\text{--}1.7$ Ga (Taylor et al., 1983; Gallet et al., 1998; Peucker-Ehrenbrink and Jahn, 2001), suggesting a relatively younger provenance than the average age of the UCC ($\sim 1.9\text{--}2.3$ Ga, Allègre and Rousseau, 1984). Glaciers may also preferentially sample younger crust given that many of the diamictites are submarine deposits formed on the margins of continents, which can be younger than continental interiors (Peucker-Ehrenbrink et al., 2010). Additional studies of diamictites, such as detrital zircon ages (Gaschnig et al., 2015 and in progress), and whole rock Hf–Nd isotope analyses are needed to evaluate the age of crust sampled by the diamictites. Another possibility for the lower estimates obtained from loess samples is that PGEs are fractionated during wind transportation owing to the larger densities of platinum-group minerals (PGM) relative to silicates.

Therefore, we suggest that the PGE abundance estimates obtained from the median PGE concentrations of the Neoproterozoic and Paleozoic diamictites and from the Quaternary loess samples are biased toward lower values, resulting from the foregoing sampling bias. This bias can be ameliorated by using the regression approach that encompasses diamictites of all ages, ranging from the Mesoarchean to Paleozoic. If an unknown element correlates with another element in rocks or sediments with all ages (not only relatively young samples, e.g., loess) for which a robust average concentration has been established for the UCC, the concentration for the unknown element obtained from the regression should be a reasonable estimate for its abundance in the modern UCC. We consider the results derived from the regression as our best estimates of the UCC PGE and Re abundances.

5.4. Secular changes in PGE-Re abundances in the UCC

Previous estimates of PGE and Re abundances in the UCC focused only on the present-day UCC composition (Esser and Turekian, 1993; Wedepohl, 1995; Schmidt

et al., 1997a; Gao et al., 1998; Peucker-Ehrenbrink and Jahn, 2001; Park et al., 2012). No studies have been conducted to assess whether PGE and Re concentrations in the UCC have varied through time. From the observed higher concentrations of first-row transition metals in averages of surface outcrops and shales, the early continental crust is hypothesized to have had a greater proportion of mafic and ultramafic lithologies than younger continental crust (Eade and Fahrig, 1973; Taylor and McLennan, 1985; Condie, 1993; Keller and Schoene, 2012; Tang et al., 2016). Similar secular changes have also been recognized in individual diamictites (Gaschnig et al., 2014) and the diamictite composites studied here (Gaschnig et al., 2016). The similarities seen in glacial diamictites and shales suggest that the former are also useful proxies for studying the composition and evolution of the UCC (Gaschnig et al., 2016). It may be expected, then, that the older diamictite composites have higher PGE concentrations than younger ones.

Figs. 2 and 3 show that PGE concentrations decrease in the diamictite composites progressing from the Mesoarchean to the Neoproterozoic, after which no change is apparent. Student's *t*-tests (Table A7) demonstrate that the older diamictite composites generally have statistically higher PGE concentrations than younger ones and that the Neoproterozoic composites are not statistically different from the Paleozoic composites. This trend is consistent with the higher concentrations of first-row transition metals and lower Al-normalized REE concentrations in the older diamictites (Figs. A2 and A4), and is also consistent with previous inference that there was a greater proportion of mafic to ultramafic lithologies in the Archean UCC compared to younger UCC. Indeed, Condie (1993) estimated that the Early Archean UCC had higher proportions of komatiite ($\sim 6\%$) and basalt ($\sim 15\%$) compared to the Proterozoic ($\sim 0\%$ and 10% , respectively) and the Phanerozoic ($\sim 0\%$ and 9% , respectively). Using the average PGE concentrations of rock types compiled from GeoRoc (Table A5), and the relative lithological proportions in the UCC estimated by Condie (1993) and Tang et al. (2016) (Table A6), one can observe the important influence of komatiite on UCC PGE concentrations. For example, adding 1% more komatiite to the Early Archean UCC results in an Ir concentration that is $\sim 10\%$ higher in Condie's model. In contrast to PGE concentrations, Re concentrations are highly variable and show no trend, likely owing to its high solubility (see Section 5.2.3).

Using the PGE data in Table A5 and the rock proportions in Table A6, we estimate the average PGE abundances for the Mesoarchean and Phanerozoic UCC (Table 4). Owing to the rarity of PGE concentration data in Proterozoic rocks, the average PGE abundances for Proterozoic UCC are not calculated here. Four points can be drawn from Table 4. First, the medians of the Mesoarchean diamictite PGE data lie between the PGE abundances of the Mesoarchean UCC calculated from Condie's model and Tang's et al. model. The diamictite Ru median is close to the Ru abundance obtained from Tang's et al., model considering the large uncertainty. And the PGE abundances for the Phanerozoic UCC obtained from Condie's

(1993) model calculation are quite similar to the medians of the Phanerozoic diamictite composites. Second, the PGE abundances in the Mesoarchean UCC obtained from diamictite composites and the model calculations are higher than those for the Phanerozoic UCC. Third, given the similarity between the results from model calculation and the composite medians for both the Mesoarchean and Phanerozoic periods, we suggest that the medians of the PGE concentrations for Paleoproterozoic and Neoproterozoic diamictite composites are representative of the PGE abundances for the Paleoproterozoic and Neoproterozoic UCC. Finally, the medians of the PGE concentrations of Neoproterozoic diamictite composites are indistinguishable from the Paleozoic diamictite composites, consistent with their similar concentrations of first-row transition metals as well as other elements (Fig. A2). These observations are consistent with the observation that the UCC composition has not changed significantly since the Archean-Proterozoic boundary (e.g., Gaschnig et al., 2016; Tang et al., 2016).

6. CONCLUSIONS

Globally-distributed glacial diamictites, which were deposited during the Mesoarchean, Paleoproterozoic, Neoproterozoic and Paleozoic eras, are good proxies not only for estimating the average composition of the present-day UCC, but also for tracking the UCC composition through time (Gaschnig et al., 2014, 2016; Li et al., 2016). The concentrations of platinum-group elements (PGEs, including Os, Ir, Ru, Pt and Pd) and the geochemically related Re, as well as $^{187}\text{Re}/^{188}\text{Os}$ and $^{187}\text{Os}/^{188}\text{Os}$ ratios reported here lead to the following conclusions:

- (1) The correlations between PGEs and Cr, Ni, and between Re and Mo, in all the diamictite composites can be used to estimate the PGE-Re abundances in the present-day UCC, with associated uncertainties ($0.059 \pm 0.016 \text{ ng/g Os}$, $0.036 \pm 0.008 \text{ ng/g Ir}$, $0.079 \pm 0.026 \text{ ng/g Ru}$, $0.80 \pm 0.22 \text{ ng/g Pt}$, $0.80 \pm 0.26 \text{ ng/g Pd}$ and $0.25 \pm 0.12 \text{ ng/g Re}$, 2σ of 10,000 bootstrapping regression results). From this, time-integrated $^{187}\text{Re}/^{188}\text{Os}$ and $^{187}\text{Os}/^{188}\text{Os}$ ratios for the UCC are calculated, yielding ratios of 20 ± 12 and 0.80 ± 0.38 (2σ), respectively.
- (2) These PGE abundance estimates are $\sim 50\% - 160\%$ higher than the estimates obtained from loess samples. We suggest two possible reasons for the difference: (1) loess preferentially samples younger UCC rocks that have lower PGE concentrations; (2) PGEs are fractionated during wind transportation during the formation of loess.
- (3) The PGE concentrations decrease in the diamictite composites progressing from the Mesoarchean to the Neoproterozoic, after which no change is apparent. This trend is consistent with the higher concentrations of first-row transition metals and lower Al-normalized REE concentrations in the older diamictites, and is also consistent with previous inference that there was a greater proportion of mafic to ultramafic lithologies in the Archean UCC compared to younger UCC.

ACKNOWLEDGEMENTS

This research was supported by the U.S. National Science Foundation (EAR-1321954 and FESD EAR-1338810), the National Nature Science Foundation of China (41373026 and 41173016), Chinese Ministry of Education (B07039) and the State Key Laboratory of Geological Processes and Mineral Resources (MSFGPMR01 and GPMR201202). We thank Richard Ash, Gregory Archer, Emily Worsham and Katherine Bermingham for help with analytical work and William McDonough, Yongsheng Liu and Huan Cui for helpful discussions. We thank Bernhard Peucker-Ehrenbrink and Ian H. Campbell for comments on a previous draft of this manuscript. Finally, we greatly appreciate the editorial work of Munir Humayun and detailed comments from Greg Ravizza, Bernhard Peucker-Ehrenbrink, and an anonymous reviewer that helped to improve the presentation.

APPENDIX A. SUPPLEMENTARY DATA

Supplementary data associated with this article can be found, in the online version, at <http://dx.doi.org/10.1016/j.gca.2016.07.004>.

REFERENCES

- Allègre C. J. and Rousseau D. (1984) The growth of the continent through geological time studied by Nd isotope analysis of shales. *Earth Planet. Sci. Lett.* **67**, 19–34.
- Anbar A. D., Creaser R. A., Papanastassiou D. A. and Wasserburg G. J. (1992) Rhenium in seawater: confirmation of generally conservative behavior. *Geochim. Cosmochim. Acta* **56**, 4099–4103.
- Barth M. G., McDonough W. F. and Rudnick R. L. (2000) Tracking the budget of Nb and Ta in the continental crust. *Chem. Geol.* **165**, 197–213.
- Becker H., Horan M. F., Walker R. J., Gao S., Lorand J. P. and Rudnick R. L. (2006) Highly siderophile element composition of the Earth's primitive upper mantle: constraints from new data on peridotite massifs and xenoliths. *Geochim. Cosmochim. Acta* **70**, 4528–4550.
- Birck J. L., Roy-Barman M. and Capmas F. (1997) Re–Os isotopic measurements at the femtomole level in natural samples. *Geostan. Newslett.* **21**, 19–27.
- Canil D. and Lacourse T. (2011) An estimate for the bulk composition of juvenile upper continental crust derived from glacial till in the North American Cordillera. *Chem. Geol.* **284**, 229–239.
- Carlson R. W. and Irving A. J. (1994) Depletion and enrichment history of subcontinental lithospheric mantle: an Os, Sr, Nd and Pb isotopic study of ultramafic xenoliths from the northwestern Wyoming Craton. *Earth Planet. Sci. Lett.* **126**, 457–472.
- Cohen A. S. and Waters F. G. (1996) Separation of osmium from geological materials by solvent extraction for analysis by thermal ionisation mass spectrometry. *Anal. Chim. Acta* **332**, 269–275.
- Colodner D., Sachs J., Ravizza G., Turekian K., Edmond J. and Boyle E. (1993) The geochemical cycle of rhenium: a renaissance. *Earth Planet. Sci. Lett.* **117**, 205–221.
- Condie K. C. (1993) Chemical composition and evolution of the upper continental crust: contrasting results from surface samples and shales. *Chem. Geol.* **104**, 1–37.
- Creaser R. A., Papanastassiou D. A. and Wasserburg G. J. (1991) Negative thermal ion mass spectrometry of osmium, rhenium and iridium. *Geochim. Cosmochim. Acta* **55**, 397–401.

- Crusius J., Calvert S., Pedersen T. and Sage D. (1996) Rhenium and molybdenum enrichments in sediments as indicators of oxic, suboxic and sulfidic conditions of deposition. *Earth Planet. Sci. Lett.* **145**, 65–78.
- Dubin A. and Peucker-Ehrenbrink B. (2015) The importance of organic-rich shales to the geochemical cycles of rhenium and osmium. *Chem. Geol.* **403**, 111–120.
- Eade K. E. and Fahrig W. F. (1973) Regional, lithological, and temporal variation in the abundances of some trace elements in the Canadian Shield. *Geol. Surv. Can. Paper* **72**, 46.
- Efron B. and Tibshirani R. J. (1993) *An Introduction to the Bootstrap*. Taylor & Francis.
- Esser B. K. and Turekian K. K. (1993) The osmium isotopic composition of the continental crust. *Geochim. Cosmochim. Acta* **57**, 3093–3104.
- Gallet S., Jahn B.-M., Van Vliet Lanoë B., Dia A. and Rossello E. (1998) Loess geochemistry and its implications for particle origin and composition of the upper continental crust. *Earth Planet. Sci. Lett.* **156**, 157–172.
- Gao S., Luo T. C., Zhang B. R., Zhang H. F., Han Y. W., Zhao Z. D. and Hu Y. K. (1998) Chemical composition of the continental crust as revealed by studies in East China. *Geochim. Cosmochim. Acta* **62**, 1959–1975.
- Gaschnig R. M., Rudnick R. L., McDonough W. F., Kaufman A. J., Hu Z. and Gao S. (2014) Onset of oxidative weathering of continents recorded in the geochemistry of ancient glacial diamictites. *Earth Planet. Sci. Lett.* **408**, 87–99.
- Gaschnig R. M., Rudnick R. L., McDonough W. F., Kaufman A. J., Vervoort J. D. and Fisher C. (2015) Insights on crustal growth from detrital zircons in ancient glacial deposits. American Geophysical Union Fall Meeting, San Francisco, pp. V51C-3053.
- Gaschnig R. M., Rudnick R. L., McDonough W. F., Kaufman A. J., Valley J. W., Hu Z., Gao S. and Beck M. L. (2016) Compositional evolution of the upper continental crust through time, as constrained by ancient glacial diamictites. *Geochim. Cosmochim. Acta* **186**, 316–343.
- Goldschmidt V. M. (1933) Grundlagen der quantitativen Geochemie. *Fortschritte der Mineralogie, Kristallographie und Petrographie* **17**, 112–156.
- Hu Z. and Gao S. (2008) Upper crustal abundances of trace elements: a revision and update. *Chem. Geol.* **253**, 205–221.
- Huber H., Koeberl C., McDonald I. and Reimold W. U. (2001) Geochemistry and petrology of Witwatersrand and Dwyka diamictites from South Africa: search for an extraterrestrial component. *Geochim. Cosmochim. Acta* **65**, 2007–2016.
- Ishikawa A., Senda R., Suzuki K., Dale C. W. and Meisel T. (2014) Re-evaluating digestion methods for highly siderophile element and ^{187}Os isotope analysis: evidence from geological reference materials. *Chem. Geol.* **384**, 27–46.
- Jaffe L. A., Peucker-Ehrenbrink B. and Petsch S. T. (2002) Mobility of rhenium, platinum group elements and organic carbon during black shale weathering. *Earth Planet. Sci. Lett.* **198**, 339–353.
- Jahn B.-M., Gallet S. and Han J. (2001) Geochemistry of the Xining, Xifeng and Jixian sections, Loess Plateau of China: eolian dust provenance and paleosol evolution during the last 140 ka. *Chem. Geol.* **178**, 71–94.
- Kamber B. S., Greig A. and Collerson K. D. (2005) A new estimate for the composition of weathered young upper continental crust from alluvial sediments, Queensland, Australia. *Geochim. Cosmochim. Acta* **69**, 1041–1058.
- Keller C. B. and Schoene B. (2012) Statistical geochemistry reveals disruption in secular lithospheric evolution about 2.5 Gyr ago. *Nature* **485**, 490–493.
- Koeberl C. and Montanari A. (2000) *Impact Stratigraphy: The Italian Record*.
- Li S., Gaschnig R. M. and Rudnick R. L. (2016) Insights into chemical weathering of the upper continental crust from the geochemistry of ancient glacial diamictites. *Geochim. Cosmochim. Acta* **176**, 96–117.
- Maier W. D., Peltonen P., McDonald I., Barnes S. J., Barnes S. J., Hatton C. and Viljoen F. (2012) The concentration of platinum-group elements and gold in southern African and Karelian kimberlite-hosted mantle xenoliths: Implications for the noble metal content of the Earth's mantle. *Chem. Geol.* **302–303**, 119–135.
- McDonough W. F. (2003) 2.15 – Compositional Model for the Earth's Core. In *Treatise on Geochemistry* (eds. H. D. Holland and K. K. Turekian). Pergamon, Oxford, pp. 547–568.
- McDonough W. F. and Sun S. S. (1995) The composition of the Earth. *Chem. Geol.* **120**, 223–253.
- McLennan S. M. (2001) Relationships between the trace element composition of sedimentary rocks and upper continental crust. *Geochim. Geophys. Geosyst.* **2** 2000GC000109.
- Meisel T. and Moser J. (2004a) Reference materials for geochemical PGE analysis: new analytical data for Ru, Rh, Pd, Os, Ir, Pt and Re by isotope dilution ICP-MS in 11 geological reference materials. *Chem. Geol.* **208**, 319–338.
- Meisel T. and Moser J. (2004b) Platinum-Group Element and Rhenium concentrations in low abundance reference materials. *Geostand. Geanal. Res.* **28**, 233–250.
- Miller C. A., Peucker-Ehrenbrink B., Walker B. D. and Marcano F. (2011) Re-assessing the surface cycling of molybdenum and rhenium. *Geochim. Cosmochim. Acta* **75**, 7146–7179.
- Morford J. L. and Emerson S. (1999) The geochemistry of redox sensitive trace metals in sediments. *Geochim. Cosmochim. Acta* **63**, 1735–1750.
- Nesbitt H. W. and Young G. M. (1996) Petrogenesis of sediments in the absence of chemical weathering: effects of abrasion and sorting on bulk composition and mineralogy. *Sedimentology* **43**, 341–358.
- Oberbeck V. R., Marshall J. R. and Aggarwal H. (1993) Impacts, tillites, and the breakup of Gondwanaland. *J. Geol.* **101**, 1–19.
- Park J.-W., Hu Z., Gao S., Campbell I. H. and Gong H. (2012) Platinum group element abundances in the upper continental crust revisited-New constraints from analyses of Chinese loess. *Geochim. Cosmochim. Acta* **93**, 63–76.
- Pearson D. G., Irvine G. J., Ionov D. A., Boyd F. R. and Dreibus G. E. (2004) Re-Os isotope systematics and platinum group element fractionation during mantle melt extraction: a study of massif and xenolith peridotite suites. *Chem. Geol.* **208**, 29–59.
- Peucker-Ehrenbrink B. and Blum J. D. (1998) Re-Os isotope systematics and weathering of Precambrian crustal rocks: implications for the marine osmium isotope record. *Geochim. Cosmochim. Acta* **62**, 3193–3203.
- Peucker-Ehrenbrink B. and Hannigan R. E. (2000) Effects of black shale weathering on the mobility of rhenium and platinum group elements. *Geology* **28**, 475–478.
- Peucker-Ehrenbrink B. and Jahn B.-M. (2001) Rhenium-osmium isotope systematics and platinum group element concentrations: loess and the upper continental crust. *Geochim. Geophys. Geosyst.* **2** 2001GC000172.
- Peucker-Ehrenbrink B., Bach W., Hart S. R., Bluszajn J. S. and Abbruzzese T. (2003) Rhenium-osmium isotope systematics and platinum group element concentrations in oceanic crust from DSDP/ODP Sites 504 and 417/418. *Geochim. Geophys. Geosyst.* **4**, 8911.
- Peucker-Ehrenbrink B., Miller M. W., Arsouze T. and Jeandel C. (2010) Continental bedrock and riverine fluxes of strontium and

- neodymium isotopes to the oceans. *Geochim. Geophys. Geosyst.* **11**, Q03016.
- Puchtel I. S., Walker R. J., Touboul M., Nisbet E. G. and Byerly G. R. (2014) Insights into early Earth from the Pt–Re–Os isotope and highly siderophile element abundance systematics of Barberton komatiites. *Geochim. Cosmochim. Acta* **125**, 394–413.
- Ravizza G. and Pyle D. (1997) PGE and Os isotopic analyses of single sample aliquots with NiS fire assay preconcentration. *Chem. Geol.* **141**, 251–268.
- Ravizza G. and Turekian K. K. (1989) Application of the ^{187}Re – ^{187}Os system to black shale geochronometry. *Geochim. Cosmochim. Acta* **53**, 3257–3262.
- Ravizza G., Turekian K. K. and Hay B. J. (1991) The geochemistry of rhenium and osmium in recent sediments from the Black Sea. *Geochim. Cosmochim. Acta* **55**, 3741–3752.
- Rehkämper M. and Halliday A. N. (1997) Development and application of new ion-exchange techniques for the separation of the platinum group and other siderophile elements from geological samples. *Talanta* **44**, 663–672.
- Rudnick R. L. and Gao S. (2003) 3.01 – Composition of the Continental Crust. In *Treatise on Geochemistry* (eds. H. D. Holland and K. K. Turekian), 1st ed. Pergamon, Oxford, pp. 1–64.
- Saal A. E., Rudnick R. L., Ravizza G. E. and Hart S. R. (1998) Re–Os isotope evidence for the composition, formation and age of the lower continental crust. *Nature* **393**, 58–61.
- Savard D., Barnes S.-J. and Meisel T. (2010) Comparison between nickel–sulfur fire assay Te co-precipitation and isotope dilution with high-pressure ashing acid digestion for the determination of platinum-group elements, rhenium and gold. *Geostand. Geognal. Res.* **34**, 281–291.
- Schmidt G., Palme H. and Kratz K.-L. (1997a) Highly siderophile elements (Re, Os, Ir, Ru, Rh, Pd, Au) in impact melts from three European impact craters (Sääksjärvi, Mien, and Dellen): Clues to the nature of the impacting bodies. *Geochim. Cosmochim. Acta* **61**, 2977–2987.
- Schmidt G., Palme H. and Kratz K.-L. (1997b) Fractionation of highly siderophile elements in the Earth's upper continental crust. In *Yearbook of Institute of Nuclear Chemistry*. Johannes Gutenberg-Universität, Mainz, Germany.
- Shaw D. M., Dostal J. and Keays R. R. (1976) Additional estimates of continental surface Precambrian shield composition in Canada. *Geochim. Cosmochim. Acta* **40**, 73–83.
- Shirey S. B. and Walker R. J. (1998) The Re–Os isotope system in cosmochemistry and high-temperature geochemistry. *Annu. Rev. Earth Planet. Sci.* **26**, 423–500.
- Sims K. W. W., Newsom H. E. and Gladney E. S. (1990) Chemical fractionation during formation of the Earth's core and continental crust: clues from As, Sb, W, and Mo. In *Origin of the Earth* (eds. H. E. Newsom, J. H. Jones and J. H. Newsom). Oxford Univ Press, pp. 291–317.
- Stein H. J., Markey R. J., Morgan J. W., Du A. and Sun Y. (1997) Highly precise and accurate Re–Os ages for molybdenite from the East Qinling molybdenum belt, Shaanxi Province. *China Econ. Geol.* **92**, 827–835.
- Tang M., Chen K. and Rudnick R. L. (2016) Archean upper crust transition from mafic to felsic marks the onset of plate tectonics. *Science* **351**, 372–375.
- Taylor S. R. and McLennan S. M. (1985) *The Continental Crust: Its Composition and Evolution*. Blackwell Scientific, Oxford.
- Taylor S. R. and McLennan S. (2008) *Planetary Crusts: Their Composition*. Cambridge University Press, New York, Origin and Evolution, p. 378.
- Taylor S. R., McLennan S. M. and McCulloch M. T. (1983) Geochemistry of loess, continental crustal composition and crustal model ages. *Geochim. Cosmochim. Acta* **47**, 1897–1905.
- Wedeppohl K. H. (1995) The composition of the continental crust. *Geochim. Cosmochim. Acta* **59**, 1217–1232.

Associate editor: Munir Humayun